Kinetic theory for a simple modeling of a phase transition: Dynamics out of local equilibrium

AUTHOR(S):

Takata, Shigeru; Matsumoto, Takuya; Hirahara, Anna; Hattori, Masanari

CITATION:

Takata, Shigeru ...[et al]. Kinetic theory for a simple modeling of a phase transition: Dynamics out of local equilibrium. Physical Review E 2018, 98(5): 052123.

ISSUE DATE:

2018-11

URL:

http://hdl.handle.net/2433/278249

Kinetic theory for a simple modeling of a phase transition: Dynamics out of local equilibrium

Shigeru Takata,[1,2,*] Takuya Matsumoto,[1] Anna Hirahara,[1] and Masanari Hattori[1,2]
[1]*Department of Aeronautics and Astronautics, Graduate School of Engineering, Kyoto University, Kyoto 615–8540, Japan*
[2]*Research Project of Fluid Science and Engineering, Advanced Engineering Research Center, Kyoto University, Kyoto 615–8540, Japan*

(Received 10 July 2018; published 20 November 2018)

This is a continuation of previous work [J. Stat. Phys., **172**, 880 (2018)] that introduces the presumably simplest model of kinetic theory for phase transition. Here the main concern is to clarify the stability of uniform equilibrium states in the kinetic regime rather than that in the continuum limit. It is found by linear stability analysis that the linear neutral curve is invariant with respect to the Knudsen number, although the transition process is dependent on the Knudsen number. In addition, numerical computations of the (nonlinear) kinetic model are performed to investigate the transition processes in detail. Numerical results show that (unexpected) incomplete transitions may happen as well as clear phase transitions.

DOI: 10.1103/PhysRevE.98.052123

I. INTRODUCTION

Recently, in Ref. [1] the first author proposed a simple kinetic model for the description of phase transitions. In this reference, the model is proposed as presumably the simplest kinetic theory model that enables one to reproduce the phase transition phenomena. A functional that decreases monotonically in time is also found for this model. In the continuum limit [2] (or the local equilibrium), it recovers the Cahn-Hilliard–type equation; based on this limiting equation, the linear stability of uniform states is studied to find a neutral curve, and numerical computations of the Cahn–Hilliard–type equation are carried out as well. The details of the phase transition in the continuum limit have been clarified.

The model is, however, not limited to the dynamics in the continuum limit, in contrast to the lattice-Boltzmann models (e.g., Refs. [3,4]), but rather aims at the dynamics in the kinetic regime (or out of local equilibrium) as in Refs. [5–8]. In the present paper, we take a further step to study the stability of uniform equilibrium states in the kinetic regime. To be more specific, we are going to study the stability problem by our kinetic theory model directly, not through the Cahn-Hilliard–type equation, and try to understand the influence of the Knudsen number. The paper is organized as follows. After summarizing our model in Sec. II, the dimensionless formulation is given in Sec. III for the clarity of similarity rule in the problem to be studied. Then, a linear stability of uniform equilibrium states is investigated in Sec. IV in a way similar to Ref. [9] but in more comprehensive way. The invariance of the neutral curve with respect to the Knudsen number is shown as well. Results of numerical computations, together with supplemental discussions, are presented in Sec. V. The paper is concluded in Sec. VI.

II. PROBLEM AND ITS FORMULATION

Consider a system (or a fluid) composed of innumerable molecules in a periodic spatial domain D:

$$\frac{\partial f}{\partial t}+\xi_i\frac{\partial f}{\partial X_i}+F_i\frac{\partial f}{\partial \xi_i}=C_*[f], \tag{1a}$$

$$C_*[f]=A(\rho)(\rho M_*-f),\quad \rho=\int f\,d\boldsymbol{\xi}, \tag{1b}$$

$$F_i=-\frac{\partial \phi}{\partial X_i},\quad \phi=\Phi_S+\Phi_L, \tag{1c}$$

$$\Phi_S=-RT_*\ln(1-b\rho)+\frac{b\rho RT_*}{1-b\rho}-2a\rho,\quad (a,b>0), \tag{1d}$$

$$\Phi_L=-\kappa\frac{\partial^2\rho}{\partial X_i^2},\quad (\kappa>0), \tag{1e}$$

$$M_*=\frac{1}{(2\pi RT_*)^{3/2}}\exp\left(-\frac{\boldsymbol{\xi}^2}{2RT_*}\right), \tag{1f}$$

where t is a time, $\boldsymbol{X}=(X_1,X_2,X_3)$ a spatial position, $\boldsymbol{\xi}=(\xi_1,\xi_2,\xi_3)$ a molecular velocity, $f(t,\boldsymbol{X},\boldsymbol{\xi})$ a velocity distribution function (VDF), $m\boldsymbol{F}=m(F_1,F_2,F_3)$ a force acting on a single molecule, with m being its mass, and ϕ a corresponding potential. The integration with respect to $\boldsymbol{\xi}$ (and its dimensionless counterpart $\boldsymbol{\zeta}$ that appears later) is carried out over its entire space $\mathbb{R}^3$, unless otherwise stated. $C_*[f]$ is the so-called collision term and plays the role of a thermal bath, driving the system toward a thermal equilibrium at a specified temperature T_* which is fixed and given. Note that the present collision term conserves neither momentum nor energy, in contrast to the usual intermolecular collision term. A is a positive function of local density ρ and $R=k_B/m$, with k_B being the Boltzmann constant. κ, a, and b are positive constants, the latter two of which are the ones occurring in the van der Waals equation of state [see (4) below]. Hence, Φ_S

*takata.shigeru.4a@kyoto-u.ac.jp

is a potential purely related to the van der Waals equation of state. In the meantime, Φ_L is a potential which comes from a collection of nonlocal attractive interactions of molecules. In the present paper, we exclusively consider the case where it can be reduced to be local and of Laplacian form by the isotropic and rapid decay assumptions in $\boldsymbol{X}$ (see Appendix A and Ref. [1] for details). We will investigate the time evolution of the system from an initial distribution

$$f(0, \boldsymbol{X}, \boldsymbol{\xi}) = f_{\rm in}(\boldsymbol{X}, \boldsymbol{\xi}), \tag{2}$$

a perturbed state from a uniform one $f = \rho_0 M_*$, with ρ_0 being the initial average density of the fluid, aiming at studying the stability of the uniform state. It is readily checked that the mass is conserved in the present system. Accordingly, the average density is constant in time.

The flow velocity $\boldsymbol{v} = (v_1, v_2, v_3)$, stress tensor p_{ij}, pressure p, and temperature T are defined as

$$\rho v_i = \int \xi_i f d\boldsymbol{\xi}, \quad p_{ij} = \int c_i c_j f d\boldsymbol{\xi} + \int \rho \Phi_S'(\rho) d\rho \delta_{ij}, \tag{3a}$$

$$p = \frac{1}{3} p_{ii}, \quad T = \frac{1}{3\rho R} \int \boldsymbol{c}^2 f d\boldsymbol{\xi}, \tag{3b}$$

where $c_i = \xi_i - v_i$, and $'$ denotes the derivative (with respect to ρ). The above definition of p is consistent with the van der Waals equation of state,

$$p = \frac{\rho RT}{1 - b\rho} - \rho^2 a, \tag{4}$$

within the isothermal approximation $T \simeq T_*$. The nonisothermal case is excluded in the present simple model, as discussed in detail in Ref. [1]. For the present system, it is shown in Ref. [1] that the following functional $\mathcal{M}$ monotonically decreases in time:

$$\begin{aligned}\mathcal{M}(t) &= \int_D \left\{ \int f \ln \frac{f}{\rho_0 M_*} d\boldsymbol{\xi} + \int \frac{\Phi_S}{RT_*} d\rho + \frac{\rho \Phi_L}{2RT_*} \right\} d\boldsymbol{X} \\ &= \int_D \left\{ \int f \ln \frac{f}{\rho_0 M_*} d\boldsymbol{\xi} + \int \frac{\Phi_S}{RT_*} d\rho \right. \\ &\quad \left. + \frac{\kappa}{2RT_*} \left(\frac{\partial \rho}{\partial X_i} \right)^2 \right\} d\boldsymbol{X}.\end{aligned}$$

Note that the second term of the above integrand is reduced to

$$\int \Phi_S d\rho = -\rho RT_* \ln(1 - b\rho) - a\rho^2,$$

under the requirement that Φ_S vanishes in the low-density limit $\rho \to 0$.

To summarize, the above model describes a nonideal gas that interacts with a thermal bath through the simple collision term. Our concern is the stability of uniform equilibrium states in such a closed nonisolated system. Incidentally, we have recently become aware of Ref. [10], which studies the stability of uniform equilibrium states by the kinetic theory. However, what is considered there is an ideal gas under a collective attractive interaction in an isolated system, and accordingly, the studied phenomenon is qualitatively different. Indeed, the details such as the linear stability analysis and its results, the derived H theorem, etc., are all different from ours.

III. DIMENSIONLESS NOTATION

For later convenience and for clarity of the similarity law for the present system, we introduce the following dimensionless notation:

$$t = \frac{L}{(2RT_*)^{1/2}} \tilde{t}, \quad X_i = L x_i, \quad \xi_i = (2RT_*)^{1/2} \zeta_i, \tag{5a}$$

$$\rho = \rho_0 \tilde{\rho}, \quad f = \frac{\rho_0}{(2RT_*)^{3/2}} \tilde{f}, \quad A(\rho) = A(\rho_0) \tilde{A}(\tilde{\rho}), \tag{5b}$$

$$\phi = 2RT_* \tilde{\phi}, \quad \Phi_S = 2RT_* \tilde{\Phi}_S, \quad \Phi_L = 2RT_* \tilde{\Phi}_L, \tag{5c}$$

$$\kappa = \frac{2RT_* L^2}{\rho_0} \tilde{\kappa}, \quad a = \frac{\tilde{a} RT_*}{\rho_0}, \quad b = \frac{\tilde{b}}{\rho_0}, \tag{5d}$$

where $\boldsymbol{x} = (x_1, x_2, x_3)$, $\boldsymbol{\zeta} = (\zeta_1, \zeta_2, \zeta_3)$, $\zeta = |\boldsymbol{\zeta}|$, and L is the characteristic length of the system, typically its period. Then the original equation and the initial condition are recast as

$$\frac{\partial \tilde{f}}{\partial \tilde{t}} + \zeta_i \frac{\partial \tilde{f}}{\partial x_i} - \frac{\partial \tilde{\phi}}{\partial x_i} \frac{\partial \tilde{f}}{\partial \zeta_i} = \frac{2}{\sqrt{\pi}} \frac{\tilde{A}(\tilde{\rho})}{\rm Kn} (\tilde{\rho} E - \tilde{f}), \tag{6a}$$

$$\tilde{f}(0, \boldsymbol{x}, \boldsymbol{\zeta}) = \tilde{f}_{\rm in}(\boldsymbol{x}, \boldsymbol{\zeta}), \tag{6b}$$

where

$$\tilde{\rho} = \int \tilde{f} d\boldsymbol{\zeta}, \quad E = \pi^{-3/2} \exp(-\zeta^2), \quad \tilde{\phi} = \tilde{\Phi}_S + \tilde{\Phi}_L, \tag{7a}$$

$$\tilde{\Phi}_S(\tilde{\rho}) = -\frac{1}{2} \ln(1 - \tilde{b}\tilde{\rho}) - \tilde{a}\tilde{\rho} + \frac{1}{2} \frac{\tilde{b}\tilde{\rho}}{1 - \tilde{b}\tilde{\rho}}, \quad (\tilde{a}, \tilde{b} > 0), \tag{7b}$$

$$\tilde{\Phi}_L = -\tilde{\kappa} \frac{\partial^2 \tilde{\rho}}{\partial x_i^2}, \quad (\tilde{\kappa} > 0), \quad \tilde{A}(\tilde{\rho}) > 0, \tag{7c}$$

and Kn is the Knudsen number defined as

$${\rm Kn} = \frac{(8RT_*/\pi)^{1/2}}{A(\rho_0) L}. \tag{7d}$$

In the above, the Strouhal number is set to be unity by the specific choice of reference time $L/(2RT_*)^{1/2}$ in (5a).

The moments of f, i.e., $v_i = (2RT_*)^{1/2} \tilde{v}_i$, $p_{ij} = \rho_0 RT_* \tilde{p}_{ij}$, $p = \rho_0 RT_* \tilde{p}$, and $T = T_* \tilde{T}$, are recast as moments of $\tilde{f}$:

$$\tilde{\rho} \tilde{v}_i = \int \zeta_i \tilde{f} d\boldsymbol{\zeta}, \quad \tilde{p}_{ij} = 2 \int \tilde{c}_i \tilde{c}_j \tilde{f} d\boldsymbol{\zeta} + 2 \int \tilde{\rho} \tilde{\Phi}_S' d\tilde{\rho}\, \delta_{ij}, \tag{8a}$$

$$\tilde{p} = \frac{1}{3} \tilde{p}_{ii}, \quad \tilde{T} = \frac{2}{3\tilde{\rho}} \int \tilde{\boldsymbol{c}}^2 \tilde{f} d\boldsymbol{\zeta}, \tag{8b}$$

where $\tilde{\boldsymbol{c}} = \boldsymbol{\zeta} - \tilde{\boldsymbol{v}}$. Furthermore, the equation of state (4) and the monotonically decreasing functional $\mathcal{M} = \rho_0 L^3 \tilde{\mathcal{M}}$ are

rewritten as

$$\tilde{p} = \frac{\tilde{\rho}\tilde{T}}{1-\tilde{b}\tilde{\rho}} - \tilde{a}\tilde{\rho}^2, \tag{9}$$

$$\begin{aligned}\tilde{\mathcal{M}}(\tilde{t}) &= \int_{\tilde{D}} \left\{ \int \tilde{f} \ln \frac{\tilde{f}}{E} d\boldsymbol{\zeta} + 2 \int \tilde{\Phi}_S d\tilde{\rho} + \tilde{\rho}\tilde{\Phi}_L \right\} d\boldsymbol{x} \\ &= \int_{\tilde{D}} \left\{ \int \tilde{f} \ln \frac{\tilde{f}}{E} d\boldsymbol{\zeta} + 2 \int \tilde{\Phi}_S d\tilde{\rho} - \tilde{\kappa}\tilde{\rho}\frac{\partial^2 \tilde{\rho}}{\partial x_i^2} \right\} d\boldsymbol{x} \\ &= \int_{\tilde{D}} \left\{ \int \tilde{f} \ln \frac{\tilde{f}}{E} d\boldsymbol{\zeta} + 2 \int \tilde{\Phi}_S d\tilde{\rho} + \tilde{\kappa}\left(\frac{\partial \tilde{\rho}}{\partial x_i}\right)^2 \right\} d\boldsymbol{x},\end{aligned} \tag{10}$$

where $\tilde{D}$ is the counterpart of D and

$$2\int \tilde{\Phi}_S d\tilde{\rho} = -\tilde{a}\tilde{\rho}^2 - \tilde{\rho}\ln(1-\tilde{b}\tilde{\rho}).$$

Note that the dimensionless mass in the domain $\tilde{D}$ is invariant in time and the average dimensionless density is unity, i.e.,

$$\frac{1}{V_{\tilde{D}}}\int_{\tilde{D}} \tilde{\rho}\, d\boldsymbol{x} = 1,$$

where $V_{\tilde{D}}$ is the volume of $\tilde{D}$.

IV. LINEAR STABILITY OF UNIFORM EQUILIBRIUM STATES

In the present section, we will study the linear stability of the uniform equilibrium state $\tilde{f} = E$. To this end, we first substitute $\tilde{f} = E + g$ into (6a) and then retain only the linear terms in g, assuming $|g| \ll E$, to have

$$\alpha\frac{\partial g}{\partial \tilde{t}} + \alpha\zeta_i\frac{\partial g}{\partial x_i} - 2\alpha\left[\tilde{\kappa}\frac{\partial^2}{\partial x_j^2} - \tilde{\Phi}_S'(1)\right]\zeta_i\frac{\partial \tilde{\rho}_g}{\partial x_i}E = \tilde{\rho}_g E - g, \tag{11}$$

where $'$ denotes the derivative (with respect to $\tilde{\rho}$) and

$$\alpha = \frac{\sqrt{\pi}}{2}\mathrm{Kn}(>0), \quad \tilde{\rho}_g = \int g\, d\boldsymbol{\zeta}.$$

Now we are going to study whether the perturbation of the form $g = \exp(\sigma\tilde{t} + i\boldsymbol{\lambda}\cdot\boldsymbol{x})h(\boldsymbol{\zeta})$, where $\boldsymbol{\lambda} = (\lambda_1, \lambda_2, \lambda_3)$, with λ_i being a positive number and $\sigma \in \mathbb{C}$, grows (i.e., $\Re\sigma > 0$) or decays (i.e., $\Re\sigma < 0$) in time, thereby finding the stability condition of the linearized system (11). Substituting it into (11) eventually yields the following identity for h [9]:

$$\begin{aligned}h = \frac{1}{\alpha\lambda}\Bigg(&\frac{S - P(\boldsymbol{\zeta}\cdot\boldsymbol{e})\alpha\lambda[Q + (\boldsymbol{\zeta}\cdot\boldsymbol{e})]}{S^2 + [Q + (\boldsymbol{\zeta}\cdot\boldsymbol{e})]^2} \\ &- \frac{i\{P(\boldsymbol{\zeta}\cdot\boldsymbol{e})S\alpha\lambda + [Q + (\boldsymbol{\zeta}\cdot\boldsymbol{e})]\}}{S^2 + [Q + (\boldsymbol{\zeta}\cdot\boldsymbol{e})]^2}\Bigg)\tilde{\rho}_h E,\end{aligned} \tag{12}$$

where $\tilde{\rho}_h = \int h d\boldsymbol{\zeta}$, $\sigma = \sigma_1 + i\sigma_2$ ($\sigma_1, \sigma_2 \in \mathbb{R}$), $\boldsymbol{e} = \boldsymbol{\lambda}/\lambda$, $\lambda = |\boldsymbol{\lambda}|$, and

$$S = \frac{1 + \alpha\sigma_1}{\alpha\lambda}, \quad P = 2[\tilde{\kappa}\lambda^2 + \tilde{\Phi}_S'(1)], \quad Q = \frac{\sigma_2}{\lambda}. \tag{13}$$

Due to the consistency, integrating both sides of (12) in $\boldsymbol{\zeta}$ leads to the following set of identities:

$$2\pi\int_0^\infty\int_0^\pi \frac{1}{\alpha\lambda}\frac{S - (\zeta\cos\theta)P\bar{Q}\alpha\lambda}{S^2 + \bar{Q}^2} E\,\zeta^2\sin\theta d\theta d\zeta = 1, \tag{14}$$

$$\int_0^\infty\int_0^\pi \frac{PS\alpha\lambda\zeta\cos\theta + \bar{Q}}{S^2 + \bar{Q}^2} E\zeta^2\sin\theta d\theta d\zeta = 0, \tag{15}$$

where $\bar{Q} \equiv Q + \zeta\cos\theta$ and θ is the angle between $\boldsymbol{\zeta}$ and $\boldsymbol{e}$, i.e., $\boldsymbol{\zeta}\cdot\boldsymbol{e} = \zeta\cos\theta$. After some manipulations, (14) is transformed into

$$(1 + PS\alpha\lambda)SI + P\alpha\lambda Q^2(I - 4J) = \frac{\alpha\lambda}{\pi}(1 + P), \tag{16}$$

while (15) is transformed into

$$Q\{(1 + PS\alpha\lambda)(I - 4J) - PS\alpha\lambda I\} = 0, \tag{17}$$

where both I and J are positive functions of Q and S, defined by

$$I(Q,S) = \int_0^\infty \left(\frac{1}{S^2 + (Q+\zeta)^2} + \frac{1}{S^2 + (Q-\zeta)^2}\right) E d\zeta,$$

$$J(Q,S) = \int_0^\infty \frac{\zeta^2 E}{\{S^2 + (Q+\zeta)^2\}\{S^2 + (Q-\zeta)^2\}} d\zeta.$$

Note that both I and J are even in Q.

Case 1. When $Q = 0$, (17) is automatically satisfied. Then, (16) with $Q = 0$ takes the form

$$2S(1 + PS\alpha\lambda)\int_0^\infty \frac{E}{S^2 + \zeta^2} d\zeta = \frac{\alpha\lambda}{\pi}(1 + P),$$

which is solved for P and is reduced to

$$P = \frac{\alpha\lambda - \sqrt{\pi}F(S)}{\sqrt{\pi}\alpha\lambda SF(S) - \alpha\lambda},$$

$$F(S) \equiv 2\sqrt{\pi}S\int_0^\infty \frac{E}{S^2 + \zeta^2} d\zeta = \exp(S^2)\{1 - \mathrm{erf}(S)\},$$

where $\mathrm{erf}(x) = (2/\sqrt{\pi})\int_0^x \exp(-s^2)ds$. Using the definitions of P and $\tilde{\Phi}_S$ [see (13) and (7b)], we obtain

$$\tilde{a} = \tilde{\kappa}\lambda^2 + \frac{1}{2}\frac{\tilde{b}(2-\tilde{b})}{(1-\tilde{b})^2} + \frac{1}{2}X, \tag{18a}$$

$$X(S, \alpha\lambda) = \frac{\alpha\lambda - \sqrt{\pi}F(S)}{\alpha\lambda\{1 - \sqrt{\pi}SF(S)\}}. \tag{18b}$$

As seen from its definition, $F(S)$ is monotonically decreasing in S from unity to zero and $x > \sqrt{\pi}F(1/x)$ for $x > 0$, while $SF(S)$ is monotonically increasing from zero to $1/\sqrt{\pi}$ in the range $0 \leqslant S < \infty$ [11]. Hence, for $S\alpha\lambda > 1$, which is equivalent to $\sigma_1 > 0$, X is monotonically increasing in S and approaches its infimum when $S \to 1/(\alpha\lambda)$:

$$X(S, \alpha\lambda) > X\left(\frac{1}{\alpha\lambda}, \alpha\lambda\right) = \frac{\alpha\lambda - \sqrt{\pi}F(1/(\alpha\lambda))}{\alpha\lambda - \sqrt{\pi}F(1/(\alpha\lambda))} = 1.$$

Therefore, when $Q = 0$, the uniform equilibrium state is unstable if

$$\tilde{a} > \frac{1}{2}\frac{\tilde{b}(2-\tilde{b})}{(1-\tilde{b})^2} + \frac{1}{2} = \frac{1}{2(1-\tilde{b})^2}.$$

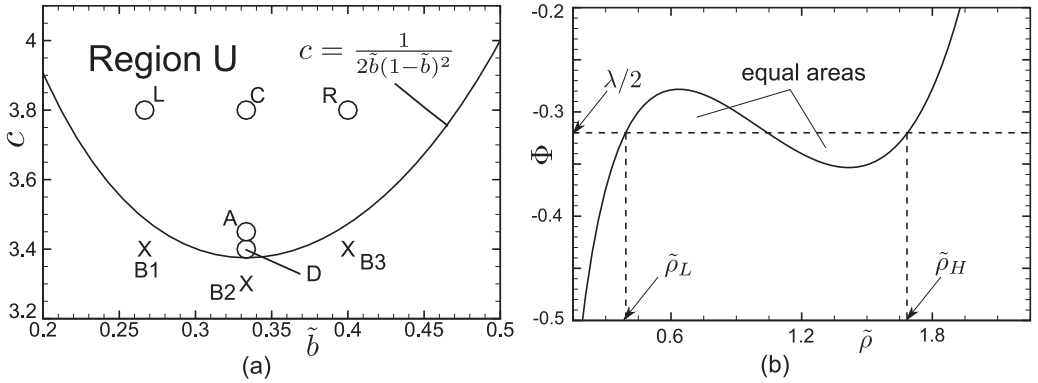

FIG. 1. Diagrams of phase transition. (a) Neutral curve of the linear stability. Markers with L, C, R, D, and A in region U indicate cases $(c, \tilde{b}) = (3.8, 4/15)$, $(3.8, 1/3)$, $(3.8, 2/5)$, $(3.4, 1/3)$, and $(3.45, 1/3)$, respectively. In region U above the neutral curve $c = 1/\{2\tilde{b}(1-\tilde{b})^2\}$, uniform equilibrium states are linearly unstable. Markers with B1, B2, and B3 indicate cases $(c, \tilde{b}) = (3.4, 4/15)$, $(3.3, 1/3)$, and $(3.4, 2/5)$, respectively. ◯ (×) indicates that the phase transition is observed (not observed) in numerical computations. Note that $\tilde{b}$ is a measure of the volume fraction of molecules to the total volume. (b) Equiarea rule for determining two densities in stationary states after phase transition. The curve is the one for case C in (a), i.e., $(c, \tilde{b}) = (3.8, 1/3)$.

Case 2. When $Q \neq 0$, the following two conditions must be satisfied simultaneously:

$$(1 + PS\alpha\lambda)SI + P\alpha\lambda Q^2(I - 4J) = \frac{\alpha\lambda}{\pi}(1 + P), \quad (19a)$$

$$(1 + PS\alpha\lambda)(I - 4J) - PS\alpha\lambda I = 0. \quad (19b)$$

In this case, using some properties of the Voigt functions [12], we can show that there is no mode that grows exponentially in time, so that uniform equilibrium states are stable for $Q \neq 0$. See Appendix B for the details of analysis.

In the long run, we conclude that there is a mode that grows exponentially in time if the following condition is satisfied [see Fig. 1(a)]:

$$c \equiv \frac{\tilde{a}}{\tilde{b}} > \frac{1}{2\tilde{b}(1-\tilde{b})^2}. \quad (20)$$

Note that this coincides with that obtained from the linear stability analysis based on the Cahn-Hilliard–type equation (see Ref. [1]; $\chi_{\rm av}$ in this reference is identical to the present $\tilde{b}$). The linear instability condition is thus invariant with respect to the Knudsen number, including the continuum limit.

In closing the present section, we make a remark that the substitution of the specific form of g is a standard way in the linear stability analysis [13] and is identical to taking the Laplace and Fourier transforms, in time and space, respectively, of Eq. (11). Since the system is linear, the principle of superposition applies; the obtained results are general accordingly. One missing point that should have been taken into account is the period of spatial domain. It does not admit the growing modes with a period longer than itself, which possibly modifies the linear neutral curve [14]. We shall come back to this point later together with numerical evidences and supplemental discussions at the end of Sec. V.

V. NUMERICAL RESULTS AND DISCUSSION

In the present section, we present some results of numerical computations of the dimensionless system (6a) for the spatially one-dimensional case in the domain $\tilde{D} = \{x_1 | 0 \leqslant x_1 < 1\}$ with the initial condition

$$\tilde{f}_{\rm in}(x_1, \boldsymbol{\zeta}) = \{1 + \epsilon \sin(2\pi x_1)\}E,$$

where $\epsilon = 0.1$. Because the form of $\tilde{f} = \psi(\tilde{t}, x_1, \zeta_1)\pi^{-1}\exp(-\zeta_2^2 - \zeta_3^2)$ is compatible to the above system and $\tilde{\rho}$ can be computed from ψ, the problem can be reduced to that of ψ, meaning a great reduction of computational cost. Once ψ is known, the functional $\tilde{\mathcal{M}}$ can be recovered as well, because $\int \tilde{f}\ln(\tilde{f}/E)d\boldsymbol{\zeta} = \int \psi \ln(\psi/E_1)d\zeta_1$, with $E_1 = \pi^{-1/2}\exp(-\zeta_1^2)$. In the actual computation, we adopt a semi-Lagrangian method (see, e.g., Refs. [15–17]) based on the Strang splitting [18] with uniform grids both in x_1 and ζ_1, where the infinite domain of ζ_1 is truncated into $|\zeta_1| \leqslant 6$. In each transport process, the 2nd–3rd weighted essentially nonoscillatory (WENO) interpolation was used. The second-order central finite difference is repeatedly applied to approximate the third-order derivative of $\tilde{\rho}$ occurring in the gradient of $\tilde{\Phi}_L$. We have also developed a finite-difference scheme and a Strang scheme with third-order polynomial spline interpolation in place of the WENO interpolation. Different methods gave consistent results as increasing grid points. We omit further details on the numerical method itself and proceed to the presentation of results.

Numerical computations were performed mainly for cases C, L, and R indicated in Fig. 1(a) by setting $\tilde{A}(\tilde{\rho}) = 1$. Figure 2 shows the time evolution of the density profile for case C for $(\sqrt{\pi}/2){\rm Kn} = 0.1$, 1, and 10 and for case B2 for $(\sqrt{\pi}/2){\rm Kn} = 1$, where $\tilde{\kappa}/\tilde{b} = 5 \times 10^{-4}$ is common among the cases. Roughly speaking, the profile in the evolution process was observed to be a little more complicated at the lower density region for smaller $\tilde{\kappa}/\tilde{b}$ and for larger Knudsen number. Figure 3 shows the evolution for $(\sqrt{\pi}/2){\rm Kn} = 1$ with different values of $\tilde{\kappa}/\tilde{b}$. It is clear from the figure, together with Fig. 2(b), that the smaller $\tilde{\kappa}/\tilde{b}$ is, the thinner the interface is. Figure 4 shows the evolution in cases L and R for $(\sqrt{\pi}/2){\rm Kn} = 1$. It is seen that the dense region is thinner for case L, while it is fatter for case R. Furthermore, the values of the density plateaux after a long time are different

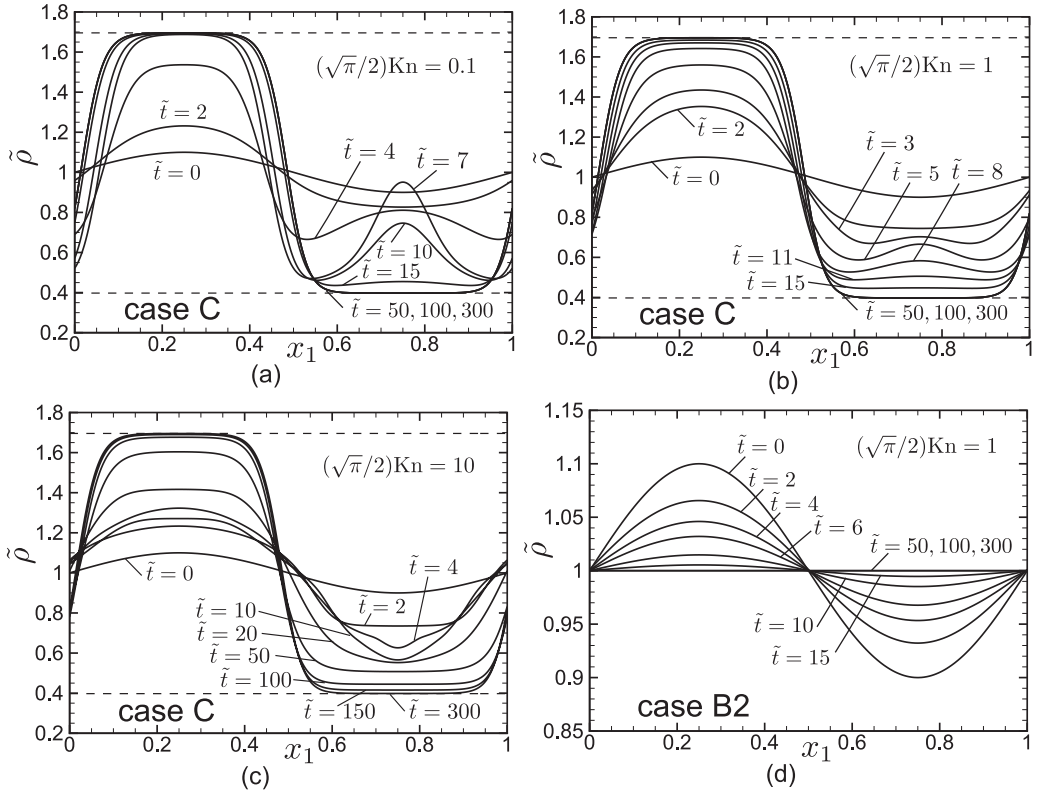

FIG. 2. Time evolution of the density profile for cases C and B2 with $\tilde{\kappa}/\tilde{b} = 5 \times 10^{-4}$. (a) $(\sqrt{\pi}/2)\mathrm{Kn} = 0.1$, (b) $(\sqrt{\pi}/2)\mathrm{Kn} = 1$, and (c) $(\sqrt{\pi}/2)\mathrm{Kn} = 10$ for case C, while (d) $(\sqrt{\pi}/2)\mathrm{Kn} = 1$ for case B2. The top and bottom dashed lines in panels (a)–(c) indicate $\tilde{\rho}_H$ and $\tilde{\rho}_L$ predicted by the equiarea rule in Fig. 1(b).

among cases L, C, and R. Further comparisons with Fig. 2 and Fig. 6(b) suggest that they are dependent on $\tilde{b}$ and c, but not on Kn nor on $\tilde{\kappa}$. Indeed, the values of the plateaus, say $\tilde{\rho}_L$ and $\tilde{\rho}_H$, can be predicted by the equiarea rule for the potential Φ (see Fig. 1(b) and Ref. [1]), which is dependent only on $\tilde{b}$ and c.

Time evolutions of the functional $\tilde{\mathcal{M}}$ are shown in Fig. 5 for various parameters. Here, the integration in space occurring in $\tilde{\mathcal{M}}$ should be understood as $\int_{\tilde{D}} \cdots d\boldsymbol{x} = \int_0^1 \cdots dx_1$. As expected, $\tilde{\mathcal{M}}$ is always monotonic and decreasing in time, while individual parts of it, say

$$\tilde{\mathcal{M}}_{\ln} \equiv \int_{\tilde{D}} \int \tilde{f} \ln \frac{\tilde{f}}{E} d\boldsymbol{\zeta} d\boldsymbol{x},$$

$$\tilde{\mathcal{M}}_A \equiv \tilde{\mathcal{M}}_{\ln} + 2 \int_{\tilde{D}} \int \tilde{\Phi}_S d\tilde{\rho} d\boldsymbol{x},$$

$$\tilde{\mathcal{M}}_L \equiv \int_{\tilde{D}} \tilde{\rho} \tilde{\Phi}_L d\boldsymbol{x} = \tilde{\kappa} \int_{\tilde{D}} \left(\frac{\partial \tilde{\rho}}{\partial x_i} \right)^2 d\boldsymbol{x} (= \tilde{\mathcal{M}} - \tilde{\mathcal{M}}_A),$$

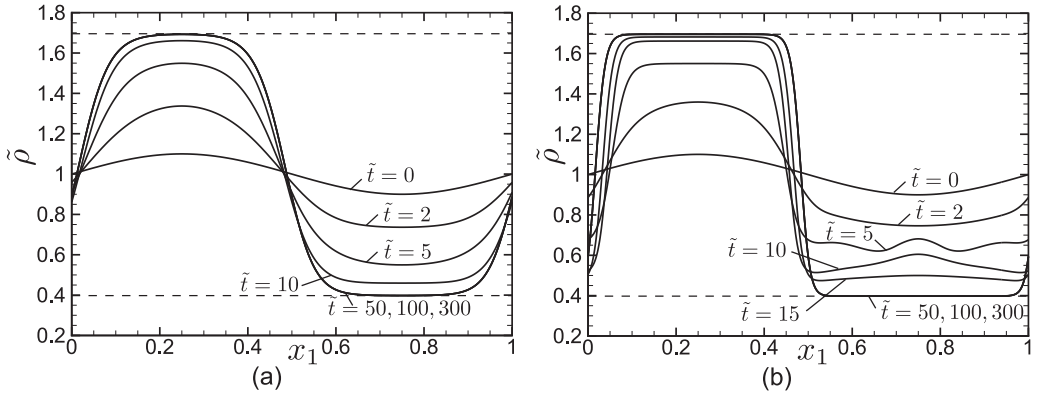

FIG. 3. Time evolution of the density profile for case C for $(\sqrt{\pi}/2)\mathrm{Kn} = 1$, (a) $\tilde{\kappa}/\tilde{b} = 1 \times 10^{-3}$ and (b) $\tilde{\kappa}/\tilde{b} = 1 \times 10^{-4}$. See also Fig. 2(b) for comparison. Top and bottom dashed lines in each panel indicate $\tilde{\rho}_H$ and $\tilde{\rho}_L$ predicted by the equiarea rule in Fig. 1(b).

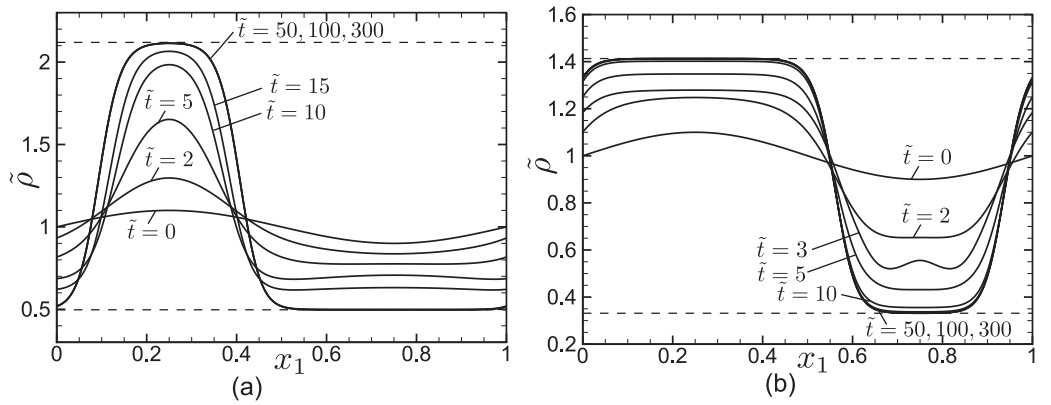

FIG. 4. Time evolution of the density profile for cases L and R for $(\sqrt{\pi}/2)\mathrm{Kn} = 1$ and $\tilde{\kappa}/\tilde{b} = 5 \times 10^{-4}$, (a) case L and (b) case R. Top and bottom dashed lines in each panel indicate $\tilde{\rho}_H$ and $\tilde{\rho}_L$ predicted by the equiarea rule in Fig. 1(b). See also Fig. 2(b) (case C) for comparison.

are not necessarily monotonic. In viewing Figs. 5(a)–5(c), it is likely that the transition takes more time for larger Knudsen numbers. In the meantime, the proper scaling that leads to the Cahn-Hilliard–type equation in the continuum limit [1] is to set the Strouhal number Sh as the order of the Knudsen number Kn. This implies that the transition will take more time as Kn becomes smaller, which seems to conflict with the above numerical evidence. Actually, however, there is no conflict. The results of additional computations for $(\sqrt{\pi}/2)\mathrm{Kn} = 0.05$ and 0.01 show that the transition indeed tends to take more time as Kn becomes much smaller, as is shown in Fig. 5(f).

Going back to the density profiles, and let us now discuss how the values of density plateaus after a long time are determined. Since $\tilde{\mathcal{M}}$ is monotonically decreasing, the system approaches its stationary state, which motivates us to consider the variational problem of $\tilde{\mathcal{M}}$ with respect to $\tilde{f}$. The variational problem of $\tilde{\mathcal{M}}$ with respect to $\tilde{f}$ followed by van Kampen's interpretation [19] leads to the equiarea rule in

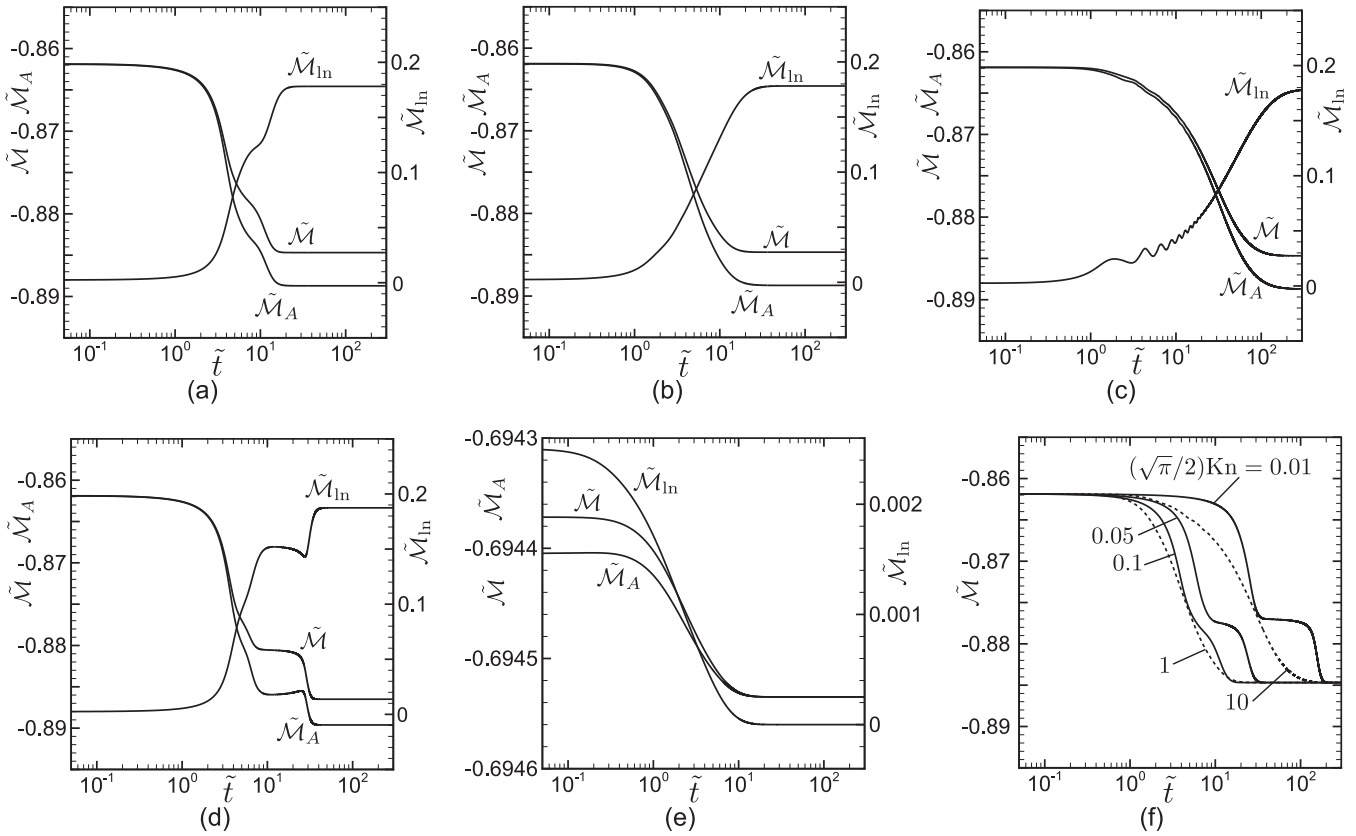

FIG. 5. Time evolution of $\tilde{\mathcal{M}}$, $\tilde{\mathcal{M}}_A$, and $\tilde{\mathcal{M}}_{\ln}$. Panels (a)–(c) are case C with $\tilde{\kappa}/\tilde{b} = 5 \times 10^{-4}$ for different Knudsen numbers: (a) $(\sqrt{\pi}/2)\mathrm{Kn} = 0.1$, (b) $(\sqrt{\pi}/2)\mathrm{Kn} = 1$, and (c) $(\sqrt{\pi}/2)\mathrm{Kn} = 10$. Panel (d) is case C with $\tilde{\kappa}/\tilde{b} = 3 \times 10^{-4}$ and $(\sqrt{\pi}/2)\mathrm{Kn} = 0.1$, while panel (e) is case B2 with $\tilde{\kappa}/\tilde{b} = 5 \times 10^{-4}$ and $(\sqrt{\pi}/2)\mathrm{Kn} = 1$. Panel (f) is case C with $\tilde{\kappa}/\tilde{b} = 5 \times 10^{-4}$ for $(\sqrt{\pi}/2)\mathrm{Kn} = 0.01, 0.05, 0.1, 1$, and 10.

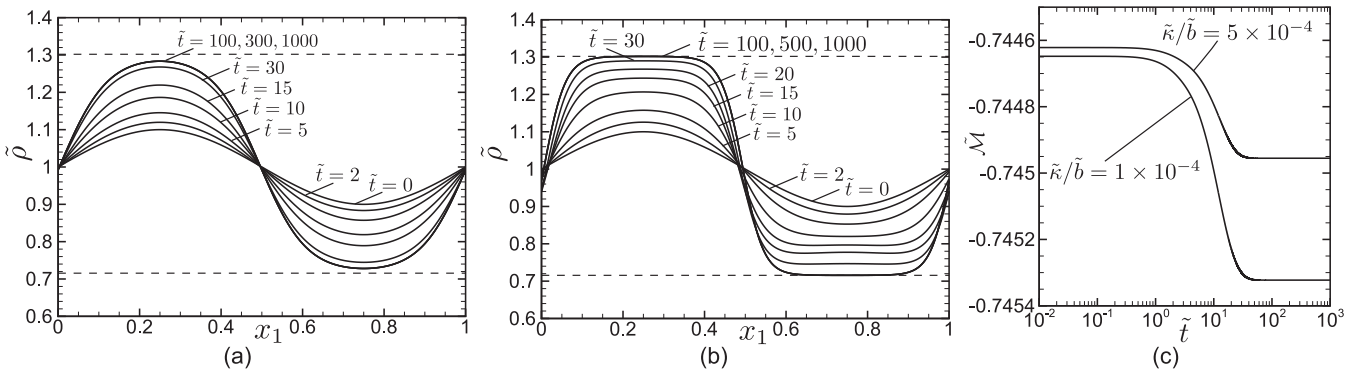

FIG. 6. Time evolution of the density and functional $\tilde{\mathcal{M}}$ in case A. (a) $\tilde{\rho}$ for $\tilde{\kappa}/\tilde{b}=5\times10^{-4}$, (b) $\tilde{\rho}$ for $\tilde{\kappa}/\tilde{b}=1\times10^{-4}$, and (c) $\tilde{\mathcal{M}}$ for both values of $\tilde{\kappa}/\tilde{b}$, where Kn is commonly set as $(\sqrt{\pi}/2)\mathrm{Kn}=1$. Top and bottom dashed lines in (a) and (b) indicate $\tilde{\rho}_H$ and $\tilde{\rho}_L$, respectively.

Fig. 1(b) for determining those values in the one-dimensional case. Let us consider the first variation of (10) under the constraint of $\int_{\tilde{D}}\tilde{\rho}d\boldsymbol{x}\equiv\int_{\tilde{D}}\int\tilde{f}d\boldsymbol{\zeta}d\boldsymbol{x}=V_{\tilde{D}}$:

$$\delta\tilde{\mathcal{M}}=\int_{\tilde{D}}\int\left\{1+\ln\frac{\tilde{f}}{E}+2\tilde{\Phi}_S(\tilde{\rho})-\tilde{\kappa}\frac{\partial^2\tilde{\rho}}{\partial x_i^2}-\tilde{\rho}\tilde{\kappa}\frac{\partial^2}{\partial x_i^2}-\lambda\right\}\times\delta\tilde{f}d\boldsymbol{\zeta}d\boldsymbol{x}$$
$$=\int_{\tilde{D}}\int\left\{1+\ln\frac{\tilde{f}}{E}+2\tilde{\Phi}_S(\tilde{\rho})-2\tilde{\kappa}\frac{\partial^2\tilde{\rho}}{\partial x_i^2}-\lambda\right\}\delta\tilde{f}d\boldsymbol{\zeta}d\boldsymbol{x},$$

where λ is the Lagrange multiplier, which is constant in $\boldsymbol{x}$ and $\boldsymbol{\zeta}$. Thus, it holds that

$$1+\ln\frac{\tilde{f}}{E}+2\tilde{\Phi}_S(\tilde{\rho})-2\tilde{\kappa}\frac{\partial^2\tilde{\rho}}{\partial x_i^2}-\lambda=0$$

at the stationary state. Then, taking into account the balance among the component terms, $\ln(\tilde{f}/E)$ is found to be independent of $\boldsymbol{\zeta}$, leading to $\tilde{f}=\tilde{\rho}E$. Hence, the above condition is reduced to

$$1+\ln\tilde{\rho}+2\tilde{\Phi}_S(\tilde{\rho})-2\tilde{\kappa}\frac{\partial^2\tilde{\rho}}{\partial x_i^2}-\lambda=0,$$

or equivalently,

$$\tilde{\kappa}\frac{\partial^2\tilde{\rho}}{\partial x_i^2}=\Phi(\tilde{\rho})-\frac{1}{2}\lambda,$$

where

$$\Phi(\tilde{\rho})\equiv\frac{1}{2}+\frac{1}{2}\ln\tilde{\rho}+\tilde{\Phi}_S$$
$$=-\tilde{a}\tilde{\rho}+\frac{1}{2}\frac{1}{1-\tilde{b}\tilde{\rho}}+\frac{1}{2}\ln\frac{\tilde{\rho}}{1-\tilde{b}\tilde{\rho}}.$$

By interpreting this condition as a motion of point mass following van Kampen (see Refs. [1,19]), we can conclude that the equiarea rule

$$\int_{\tilde{\rho}_L}^{\tilde{\rho}_H}\Phi(r)dr=\frac{\lambda}{2}(\tilde{\rho}_H-\tilde{\rho}_L)\tag{21a}$$

with

$$\Phi(\tilde{\rho}_H)=\Phi(\tilde{\rho}_L)=\frac{\lambda}{2}\tag{21b}$$

applies, where $\tilde{\rho}_H$ and $\tilde{\rho}_L$ respectively denote larger and smaller values of density plateaux. This rule determines $\tilde{\rho}_H$ and $\tilde{\rho}_L$ as sketched in Fig. 1(b). Note that the curve of Φ is dependent only on $\tilde{b}$; once $\tilde{a}$ (or c) is fixed, so are the values of $\tilde{\rho}_H$ and $\tilde{\rho}_L$.

Finally, we shall remark on a couple of unexpected phenomena that were found numerically in the above neighborhood of the neutral curve. First, a clear separation of plateaux and interfaces might not be achieved in the above neighborhood of the neutral curve, if $\tilde{\kappa}/\tilde{b}$ is not sufficiently small. Figure 6(a) demonstrates such an example (case A, $\tilde{\kappa}/\tilde{b}=5\times10^{-4}$ and $(\sqrt{\pi}/2)\mathrm{Kn}=1$). In the case, the phase transition is incomplete and the evolution ceases with a smooth profile as in Fig. 6(a). In the meantime, the interface ought to be thinner for smaller $\tilde{\kappa}$ and the transition is more likely to be completed. Indeed, for case A with $\tilde{\kappa}/\tilde{b}=1\times10^{-4}$ and $(\sqrt{\pi}/2)\mathrm{Kn}=1$, a clear separation of different plateaux and interfaces is observed, as in Fig. 6(b). Then, the equiarea rule revives for the prediction of the values of density plateaux. Second, a uniform equilibrium state can be stable in the above neighborhood of the neutral curve as shown in Fig. 7(b), which would be more striking. This is, however, understandable, if we take into account the domain periodicity in the linear stability analysis in Sec. IV. As we have already mentioned at the end of Sec. IV, the periodicity of space domain has not been taken into account in the derivation of the unstable condition (20). In order to take it into account, we need to go back to (18) and to use that the admitted modes should meet the condition $\lambda>2\pi$. Then, the unstable condition is found to take the following modified form:

$$c>\frac{1}{2\tilde{b}(1-\tilde{b})^2}+\frac{\tilde{\kappa}}{\tilde{b}}(2\pi)^2.\tag{22}$$

It is readily seen that all the cases for which the transition, including the *incomplete* one, is observed meet the above condition, while all the cases for which the uniform equilibrium state is observed stable do not. For instance, case D with $(\sqrt{\pi}/2)\mathrm{Kn}=0.1$ shown in Fig. 7(a) is in a modified linear unstable region when $\tilde{\kappa}/\tilde{b}=1\times10^{-4}$. It is, however, shifted indeed into the modified linear stable region by changing the value of $\tilde{\kappa}/\tilde{b}$ to 1×10^{-3}. Then the uniform equilibrium state becomes stable, as is demonstrated numerically in Fig. 7(b). By the same reason, in case D with $\tilde{\kappa}/\tilde{b}=1\times10^{-3}$, the

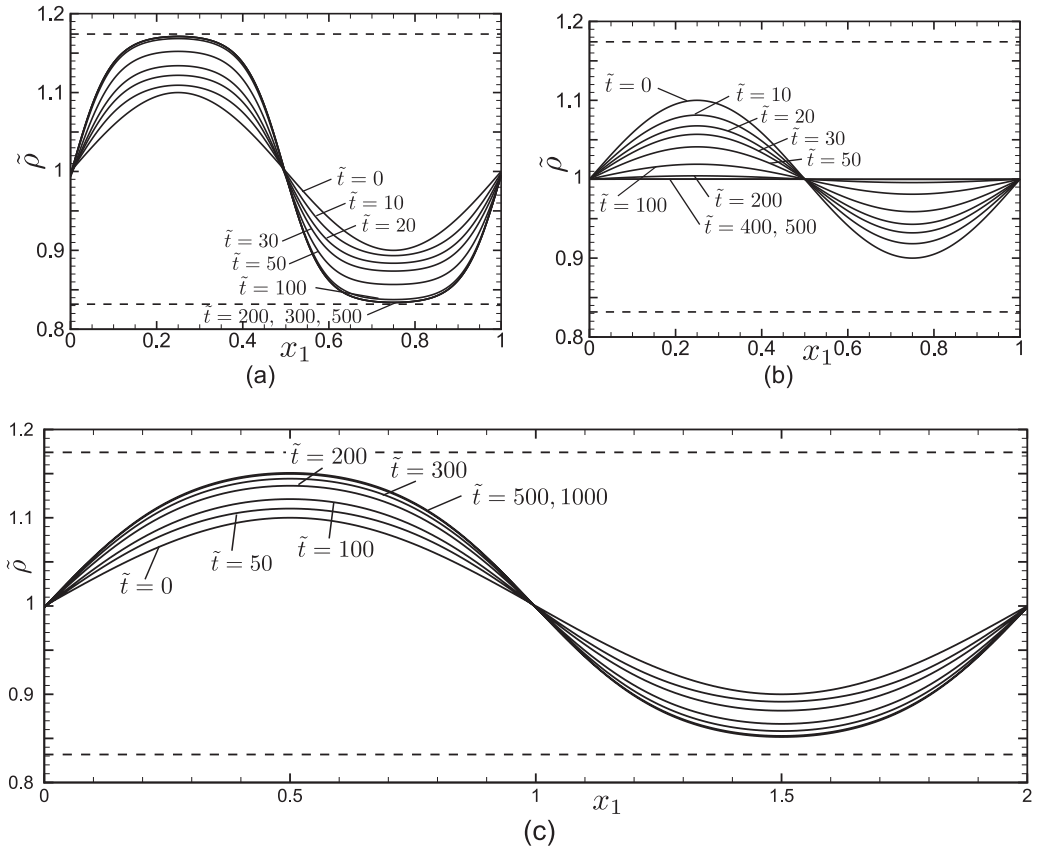

FIG. 7. Influence of the domain periodicity: time evolution of the density profile for case D for $(\sqrt{\pi}/2)\mathrm{Kn} = 0.1$. (a) $\tilde{\kappa}/\tilde{b} = 1 \times 10^{-4}$ with period 1, (b) $\tilde{\kappa}/\tilde{b} = 1 \times 10^{-3}$ with period 1, (c) $\tilde{\kappa}/\tilde{b} = 1 \times 10^{-3}$ with period 2. In (c), the sinusoidal initial perturbation has a period 2. Top and bottom dashed lines in each panel indicate $\tilde{\rho}_H$ and $\tilde{\rho}_L$, respectively.

uniform equilibrium state becomes unstable if the domain period is doubled. It is because the upper bound of the admitted mode period is accordingly doubled; consequently, the unstable condition becomes

$$c > \frac{1}{2\tilde{b}(1-\tilde{b})^2} + \frac{\tilde{\kappa}}{\tilde{b}}\pi^2,$$

and case D falls into a new unstable region. It is demonstrated numerically in Fig. 7(c).

VI. CONCLUSION

In the present paper, we have investigated the stability of uniform equilibrium states in the kinetic regime. The linear stability analysis shows that the linear unstable condition is the same as that of the Cahn-Hilliard–type equation in Ref. [1], irrespective of the Knudsen number. The condition is not affected by κ (or $\tilde{\kappa}$) as well, the measure of the collective long-range interaction effect occurring in Φ_L (or $\tilde{\Phi}_L$). By numerical computations we have indeed observed the phase transition after perturbing uniform equilibrium states that lie above the neutral curve in the diagram of Fig. 1(a). We did not observe unstable uniform equilibrium states below this curve [cases B1, B2, and B3 in Fig. 1(a)], although the computed cases are limited. The numerical results show that κ (or $\tilde{\kappa}$) mainly affects the thickness of the interface between different phases; the smaller κ (or $\tilde{\kappa}$) is, the thinner the interface is. The Knudsen number affects the transition process but does not affect the values of density plateaux at the final states. They are determined by another diagram, i.e., the equiarea rule, in Fig. 1(b), as long as the interface is thin enough for the clear separation of different plateaux to emerge. The numerical results further show that the functional $\mathcal{M}$ (or $\tilde{\mathcal{M}}$) indeed monotonically decreases as predicted in Ref. [1], though its component terms are not necessarily monotonic in the transition process.

ACKNOWLEDGMENTS

The present work was supported in part by JSPS KAKENHI Grant No. 17K18840.

APPENDIX A: ON THE FORM OF Φ_L AND Φ_S

Here we repeat the explanation about the specific form of Φ_L and Φ_S briefly for the sake of convenience of the reader, although it has already been given in Ref. [1].

The self-consistent force potential ϕ, which is of the conventional Vlasov type, is split into attractive and repulsive parts. The attractive part, Φ_A, is of long range, while the repulsive part, Φ_R, is of short range and is a function of the local density ρ. By the latter and a part of the former, we intend to reproduce a nonideal gas feature under the isothermal approximation, which is represented by the potential Φ_S.

An excluding effect by the repulsive force is usually included in the collision term with detailed collision dynamics, like in the Enskog equation. Hence, the simplification by combining the mean-field repulsive potential and the simplified role of the collision term is the main difference from the existing model [5,6].

The attractive mean field is expressed by

$$\begin{aligned} m\Phi_A(t,\boldsymbol{X}) &= \int_{\mathbb{R}^3} \Psi(|\boldsymbol{r}|)\{\rho(t,\boldsymbol{X}+\boldsymbol{r})-\rho(t,\boldsymbol{X})\}d\boldsymbol{r} \\ &\quad + \int_{\mathbb{R}^3} \Psi(|\boldsymbol{r}|)d\boldsymbol{r}\rho(t,\boldsymbol{X}) \\ &\equiv m\Phi_L[\rho] + \int_{\mathbb{R}^3} \Psi(|\boldsymbol{r}|)d\boldsymbol{r}\rho(t,\boldsymbol{X}), \end{aligned} \tag{A1}$$

where $m\Psi$ is the attractive intermolecular potential and is assumed to be isotropic. Here Φ_L may be considered as a contribution from the long tail to the total attractive potential. The subtracted part $\int_{\mathbb{R}^3}\Psi(|\boldsymbol{r}|)d\boldsymbol{r}\ \rho(t,\boldsymbol{X})$ will be combined with the repulsive part Φ_R to form the residue $m\Phi_S$ in the total self-consistent potential $m\phi$,

$$m\Phi_S = m\Phi_R + \left\{\int_{\mathbb{R}^3}\Psi(|\boldsymbol{r}|)d\boldsymbol{r}\right\}\rho(t,\boldsymbol{X}), \tag{A2}$$

the functional form of which is to be determined from the van der Waals equation of state. Since Φ_S is of short range, we are motivated to treat this as a local (or internal) variable, thereby related to the stress tensor (and the static pressure) through the momentum balance equation. This is the key idea behind our phenomenological determination of Φ_S from the equation of state. (See Sec. 3 of Ref. [1] for the specific construction.)

When Ψ decays fast in the system size as usually expected, the variation of ρ is moderate in that scale and the Taylor expansion is allowed to yield

$$\begin{aligned} \Phi_L[\rho](t,\boldsymbol{X}) &= \frac{1}{m}\int_{\mathbb{R}^3}\Psi(|\boldsymbol{r}|)\{\rho(t,\boldsymbol{X}+\boldsymbol{r})-\rho(t,\boldsymbol{X})\}d\boldsymbol{r} \\ &= \frac{1}{m}\int_{\mathbb{R}^3}\Psi(|\boldsymbol{r}|)\left\{r_i\frac{\partial}{\partial X_i}\rho(t,\boldsymbol{X})\right. \\ &\quad \left. + \frac{1}{2}r_ir_j\frac{\partial^2}{\partial X_i\partial X_j}\rho(t,\boldsymbol{X})+\cdots\right\}d\boldsymbol{r} \\ &\simeq \frac{1}{6m}\int_{\mathbb{R}^3}\Psi(|\boldsymbol{r}|)r^2d\boldsymbol{r}\frac{\partial^2}{\partial X_i^2}\rho(t,\boldsymbol{X}) \\ &\equiv -\kappa\frac{\partial^2}{\partial X_i^2}\rho(t,\boldsymbol{X}). \end{aligned} \tag{A3}$$

Here $\kappa > 0$, since Ψ is attractive. The reduction from the second to the last line is a consequence of the isotropic assumption on Ψ. This ends the derivation of the Laplacian form of Φ_L.

APPENDIX B: STABILITY ANALYSIS FOR CASE 2: $Q \neq 0$

When $Q \neq 0$, the following two conditions must be satisfied simultaneously:

$$(1+PS\alpha\lambda)SI + P\alpha\lambda Q^2(I-4J) = \frac{\alpha\lambda}{\pi}(1+P), \tag{B1a}$$

$$(1+PS\alpha\lambda)(I-4J) - PS\alpha\lambda I = 0. \tag{B1b}$$

Because I and $I-4J$ can be converted into the Voigt functions U and V as

$$\pi S^2 I(Q,S) = U\left(\frac{Q}{S},\frac{1}{4S^2}\right), \tag{B2a}$$

$$\pi SQ[I(Q,S)-4J(Q,S)] = V\left(\frac{Q}{S},\frac{1}{4S^2}\right), \tag{B2b}$$

the above conditions are recast as

$$(1+PS\alpha\lambda)U + P\alpha\lambda QV = S\alpha\lambda(1+P), \tag{B3}$$

$$(1+PS\alpha\lambda)V - P\alpha\lambda QU = 0, \tag{B4}$$

where the Voigt functions U and V are defined for $x \in \mathbb{R}$ and $t > 0$ as [12]

$$U(x,t) \equiv \frac{1}{\sqrt{4\pi t}}\int_{-\infty}^{\infty}\frac{1}{1+y^2}\exp\left(-\frac{(x-y)^2}{4t}\right)dy,$$

$$V(x,t) \equiv \frac{1}{\sqrt{4\pi t}}\int_{-\infty}^{\infty}\frac{y}{1+y^2}\exp\left(-\frac{(x-y)^2}{4t}\right)dy.$$

Obviously both U and V are positive for $x > 0$. Moreover, $xU(x,\cdot) - V(x,\cdot)$ is positive for $x > 0$, thanks to (B2). Solving both conditions for P tells that

$$\frac{S\alpha\lambda - U}{S\alpha\lambda(U+QV/S-1)} = -\frac{V}{S\alpha\lambda(V-UQ/S)}, \tag{B5}$$

which is solved to give

$$S\alpha\lambda = 0_+, \quad \frac{qU^2+qV^2-V}{qU-V},$$

where $q \equiv Q/S$ and the arguments of U and V are q and $1/(4S^2)$. In order for the uniform equilibrium state to be unstable, the second solution in the above should be larger than unity, namely,

$$\frac{qU^2+qV^2-V}{qU-V} > 1. \tag{B6}$$

We will show that this is impossible.

Because the condition (B1) is even in Q, we may assume $Q > 0$ (or $q > 0$) without loss of generality. Because $qU - V > 0$, the condition (B6) is reduced to

$$qU^2+qV^2-V > qU-V, \quad \text{i.e., } U^2+V^2-U > 0.$$

Now let us consider the function

$$H(q,S) \equiv U\left(q,\frac{1}{4S^2}\right)^2 + V\left(q,\frac{1}{4S^2}\right)^2 - U\left(q,\frac{1}{4S^2}\right).$$

On one hand, we have

$$\lim_{q\downarrow 0} H(q,S) = \sqrt{\pi}SF(S)\{\sqrt{\pi}SF(S)-1\} < 0, \tag{B7}$$

because $\lim_{q\downarrow0} V(q,\frac{1}{4S^2}) = 0$ and $\lim_{q\downarrow0} U(q,\frac{1}{4S^2}) = \frac{S}{\sqrt{\pi}}\int_{-\infty}^{\infty}\frac{1}{1+y^2}\exp(-S^2y^2)dy = \sqrt{\pi}S\exp(S^2)\{1-\mathrm{erf}(S)\} = \sqrt{\pi}SF(S)$. On the other hand, because the Voigt functions are known to satisfy the following equations:

$$V(x,t) = xU(x,t) + 2t\frac{\partial U(x,t)}{\partial x},$$

$$U(x,t) = 1 - xV(x,t) - 2t\frac{\partial V(x,t)}{\partial x},$$

we have

$$\begin{aligned}\frac{\partial H}{\partial q} &= 2U\frac{\partial U}{\partial q} + 2V\frac{\partial V}{\partial q} - \frac{\partial U}{\partial q}\\ &= 4US^2(V-qU)+4VS^2(1-qV-U)-(V-qU)2S^2\\ &= 2S^2\{-2q(U^2+V^2)+V+qU\}\\ &= 2S^2\{-2qH-qU+V\},\end{aligned}$$

which is solved to yield

$$\begin{aligned}H(q,S) &= H(0,S)e^{-2S^2q^2}\\ &\quad + \int_0^q 2S^2\left\{V\left(r,\frac{1}{4S^2}\right) - rU\left(r,\frac{1}{4S^2}\right)\right\}\\ &\quad \times e^{-2S^2(q^2-r^2)}dr < H(0,S)e^{-2S^2q^2} < 0,\end{aligned}$$

because of $rU(r,\cdot) - V(r,\cdot) > 0$ and (B7). Hence, any mode with $Q \neq 0$ is shown not to grow exponentially, and accordingly, the uniform equilibrium state is linear stable.

[1] S. Takata and T. Noguchi, A simple kinetic model for the phase transition of the van der Waals fluid, J. Stat. Phys. **172**, 880 (2018).

[2] It is rather conventional in the kinetic theory community to use this terminology for the limit of frequent collisions. This limit is sometimes further classified into the fluid-dynamic (or Navier-Stokes), diffusion (or diffusive), and acoustic (or Euler) limits, depending on the resulting set of equations described by the macroscopic quantities. We follow these conventions in the present paper.

[3] M. R. Swift, E. Orlandini, W. R. Osborn, and J. M. Yeomans, Lattice Boltzmann simulations of liquid-gas and binary fluid systems, Phys. Rev. E **54**, 5041 (1996).

[4] G. Gonnella, A. Lamura, and V. Sofonea, Lattice Boltzmann simulation of thermal nonideal fluids, Phys. Rev. E **76**, 036703 (2007).

[5] M. Grmela, Kinetic equation approach to phase transitions, J. Stat. Phys. **3**, 347 (1971).

[6] A. Frezzotti, L. Gibelli, and S. Lorenzani, Mean field kinetic theory description of evaporation of a fluid into vacuum, Phys. Fluids **17**, 012102 (2005).

[7] K. Kobayashi, K. Ohashi, and M. Watanabe, Numerical analysis of vapor-liquid two-phase system based on the Enskog-Vlasov equation, AIP Conf. Proc. **1501**, 1145 (2012).

[8] A. Frezzotti and P. Barbante, Kinetic theory aspects of non-equilibrium liquid-vapor flows, Mech. Eng. Rev. **4**, 16-00540 (2017).

[9] B. Perthame and S. Yasuda, Stiff-response-induced instability for chemotactic bacteria and flux-limited Keller-Segel equation, Nonlinearity **31**, 4065 (2018).

[10] E. S. Benilov and M. S. Benilov, Semiphenomenological model for gas-liquid phase transitions, Phys. Rev. E **93**, 032148 (2016).

[11] In order to show that $SF(S)$ is monotonically increasing, let us consider $G(x) \equiv \sqrt{\pi}\{1-\mathrm{erf}(x)\} - \frac{2x}{1+2x^2}\exp(-x^2)$. Then by direct calculation it is seen that $G' < 0$. Since $G(0) = \sqrt{\pi}$ and $G(\infty) = 0$, $G > 0$ for $0 \leqslant x < \infty$. This leads to $\sqrt{\pi}F(x) > \frac{2x}{1+2x^2}$, so that $\sqrt{\pi}xF(x) - 1 > -\frac{1}{1+2x^2}$. Therefore, $(xF)' = F + xF' = F + 2x(xF - \frac{1}{\sqrt{\pi}}) > F - \frac{2}{\sqrt{\pi}}\frac{x}{1+2x^2} > 0$, which concludes that $SF(S)$ is monotonically increasing in $0 \leqslant S < \infty$. The limiting value of $xF(x)$ as $x \to \infty$ can be found in the literature.

[12] *NIST Handbook of Mathematical Functions*, edited by F. W. J. Olver, D. W. Lozier, R. F. Boisvert, and C. W. Clark (Cambridge University Press, New York, 2010), Sec. 7.19; *NIST Digital Library of Mathematical Functions* (https://dlmf.nist.gov/7.19).

[13] S. Chandrasekhar, *Hydrodynamic and Hydromagnetic Stability* (Dover, New York, 1981).

[14] The period of space domain does not affect the result and discussions for $Q \neq 0$.

[15] J.-M. Qiu and A. Christlieb, A conservative high order semi-Lagrangian WENO method for the Vlasov equation, J. Comp. Phys. **229**, 1130 (2010).

[16] L. Einkemmer and A. Ostermann, Convergence analysis of Strang splitting for Vlasov-type equations, SIAM J. Numer. Anal. **52**, 140 (2014).

[17] M. Groppi, G. Russo, and G. Stracquadanio, High order semi-Lagrangian methods for the BGK equation, Commun. Math. Sci. **14**, 389 (2016).

[18] The scheme is composed of five steps: (i) transport in space for a half time step, (ii) that in molecular velocity space for the same time step, (iii) collision for a full time step, (iv) transport in molecular velocity space for a half time step, and (v) that in space for the same time step. Then the solution after the full time step is obtained with second-order accuracy in time.

[19] N. G. van Kampen, Condensation of a classical gas with long-range attraction, Phys. Rev. **135**, A362 (1964).